Three-terminal quantum-dot refrigerators

Yanchao Zhang, Guoxing Lin, and Jincan Chen*
Department of Physics, Xiamen University, Xiamen 361005, People's Republic of China
(Received 21 January 2015; published 13 May 2015)

Based on two capacitively coupled quantum dots in the Coulomb-blockade regime, a model of three-terminal quantum-dot refrigerators is proposed. With the help of the master equation, the transport properties of steady-state charge current and energy flow between two quantum dots and thermal reservoirs are revealed. It is expounded that such a structure can be used to construct a refrigerator by controlling the voltage bias and temperature ratio. The thermodynamic performance characteristics of the refrigerator are analyzed, including the cooling power, coefficient of performance (COP), maximum cooling power, and maximum COP. Moreover, the optimal regions of main performance parameters are determined. The influence of dissipative tunnel processes on the optimal performance is discussed in detail. Finally, the performance characteristics of the refrigerators operated in two different cases are compared.

DOI: 10.1103/PhysRevE.91.052118 PACS number(s): 05.60.Gg, 05.70.−a, 73.23.−b, 73.50.Lw

I. INTRODUCTION

Thermoelectric materials can convert unused waste heat to electricity based on the Seebeck effect or use electricity to refrigeration based on the Peltier effect. Due to the discovery of new thermoelectric materials with significantly higher thermoelectric figures of merit (ZT), the thermoelectric field went through a revival in the early 1990s [1,2]. In particular, investigations on the thermoelectric effects of nanothermoelectric devices have attracted considerable interest due to their importance in developing miniaturized devices, which help to utilize energy resources at the microscopic scale [3,4]. Such nanothermoelectric devices based on thermoelectric phenomena can be used for several applications, including the power generation, refrigeration, and temperature measurement [3]. It was pointed out that compared to bulk structures made from same materials, structures of reduced dimension can give rise to an increased thermoelectric figure of merit ZT [5,6] and that sharp spectral features can improve thermoelectric performances characterized by a high value of ZT in materials with a delta-like density of states [7]. Furthermore, it was reported that the Carnot efficiency can be reached for reversible electron transport between two reservoirs at different temperatures and chemical potentials by using a sharply tuned energy filter for which the electron density is the same in both reservoirs [8,9].

In particular, zero-dimensional (0D) systems, such as quantum dots that naturally provide these sharp spectral features, are weakly coupled to electron reservoirs and can be designed as ideal energy filters [9]. Hence, there are many investigations of the quantum dot thermoelectric devices because quantum dots can be applied to the high-potential solid-state energy conversion devices [10–15]. Experimentally, thermoelectric effect has been studied for both open quantum dots [16,17] and Coulomb-blockade dots [18–20]. In 1993, Edwards *et al.* presented a quantum dot refrigerator, which utilizes the discrete energy levels of quantum dots [21,22]. The refrigeration in quantum dot is realized by using tunneling structures with sharp energy features and filtering the energy of the current-carrying electrons [23]. The thermoelectric properties of two capacitively coupled quantum dots in the Coulomb-blockade regime in a three-terminal nanosized structure thermoelectric system were first analyzed by Sánchez *et al.* [24]. They showed that such a system can be used to transform a part of the heat flowing from a hot reservoir into electric current. Furthermore, they demonstrated that a three-terminal heat engine can act as an ideal thermal-to-electric energy converter that can reach the Carnot efficiency. Recently, Pekola *et al.* proposed a remarkably simple electronic refrigerator based on the Coulomb barrier for single-electron tunneling and provided an interesting possibility for realizing a Coulomb blockade enabled refrigerator [25]. On the basis of the previous works, we propose a three-terminal quantum-dot refrigerator based on two capacitively coupled quantum dots in the Coulomb-blockade regime. It should be pointed out that when the irreversibility is taken into account, the refrigeration model proposed here is not the simple reverse operation of the heat engine model described in Ref. [24]; it includes the contribution of some undesired processes neglected in Ref. [24] and may be directly used to discuss the optimal design problem of parameters, which was not considered in Ref. [24]. Thus, the main focus in this paper is to analyze the thermodynamic performance characteristics and optimal performance of three-terminal quantum-dot refrigerators. The influence of the main parameters, include the dissipation factor, voltage bias, and temperature ratio on the performance are discussed in detail.

This paper is organized as follows. In Sec. II, we briefly describe the model and basic physical theory of a three-terminal quantum-dot nanostructure. In Sec. III, we investigate the charge and energy transport properties. In Sec. IV, the general performance characteristics and optimization of the three-terminal quantum-dot refrigerator are discussed in detail. And the performance characteristics of refrigerators operated in the cases of $T_s > T_g$ and $T_g > T_s$ are compared, where T_s and T_g are the temperature of two heat reservoirs. Finally, the important results of this work are summarized in Sec. V.

II. MODEL AND THEORY

A model of three-terminal quantum-dot refrigerators is illustrated in Fig. 1(a), where the system consists of three

*Electronic address: jcchen@xmu.edu.cn

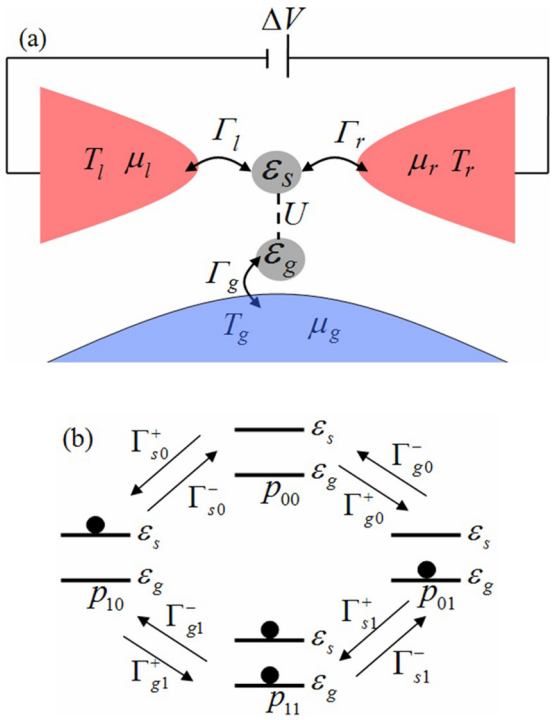

FIG. 1. (Color online) (a) The schematic diagram of a three-terminal quantum-dot refrigerator. (b) Available transition for the situation described in (a).

independent heat reservoirs and two quantum dots. The conductor dot s is embedded between two conductor reservoirs via two tunnel contacts, which permit particle and energy exchange between the left reservoir at temperature T_l and chemical potential μ_l and the right reservoir at temperature T_r and chemical potential μ_r. The gate dot g is coupled to a single-gate reservoir with temperature T_g and chemical potential μ_g. U is the long-range Coulomb interaction between the electrons of the conductor dot s and the gate dot g. The transition rates Γ_l, Γ_r, and Γ_g describe the tunneling of the electrons between the reservoirs and two quantum dots. If the two quantum dots are far from each other, they can be bridged to obtain a strong coupling and at the same time ensure good thermal isolation between the conductor reservoir and the gate reservoir [26,27]. Thus, quantum dots s and g are capacitively coupled to each other and interact only though the long-range Coulomb force such that they can only exchange energy but no particles. Quantum dots s and g have their respective single energy levels ε_s and ε_g. Because Coulomb interactions prevent two electrons to be present at one energy level at the same time, so the single energy level ε_s or ε_g can be occupied only by zero or one electron. The dynamical evolution of such a system is characterized by four quantum states $|n_s n_g\rangle$ with respective probabilities $p_{n_s n_g}$, where the electron occupation numbers $\{n_s,n_g\}$ of quantum dots s and g are equal to $\{0,0\}$, $\{0,1\}$ $\{1,0\}$, and $\{1,1\}$, respectively, as shown in Fig. 1(b), where transition rates $\Gamma^{\pm}_{\alpha n}$ describe the tunneling of electrons into (+) or out (−) one quantum dot through barrier α ($\alpha = s,g$) when the other quantum dot has n ($n = 0,1$) electrons.

In sequential tunneling approximation ($\hbar\Gamma \ll k_B T$), the broadening of energy levels can be neglected and the transmission through tunnel barriers is defined by sequential tunneling of a single electron. Thus, the evolution of the occupation probabilities of quantum states is described by master equation [28–30]

$$\begin{pmatrix} \dot{p}_{00} \\ \dot{p}_{10} \\ \dot{p}_{01} \\ \dot{p}_{11} \end{pmatrix} = \begin{pmatrix} -\Gamma^+_{s0} - \Gamma^+_{g0} & \Gamma^-_{s0} & \Gamma^-_{g0} & 0 \\ \Gamma^+_{s0} & -\Gamma^-_{s0} - \Gamma^+_{g1} & 0 & \Gamma^-_{g1} \\ \Gamma^+_{g0} & 0 & -\Gamma^+_{s1} - \Gamma^-_{g0} & \Gamma^-_{s1} \\ 0 & \Gamma^+_{g1} & \Gamma^+_{s1} & -\Gamma^-_{s1} - \Gamma^-_{g1} \end{pmatrix} \begin{pmatrix} p_{00} \\ p_{10} \\ p_{01} \\ p_{11} \end{pmatrix}, \tag{1}$$

where $\Gamma^{\pm}_{sn} = \Gamma^{\pm}_{\ln} + \Gamma^{\pm}_{rn}$, $(s = l,r)$. The transition rates $\Gamma^{\pm}_{\alpha n}$ are, respectively, given by

$$\Gamma^+_{\alpha n} = \gamma_{\alpha n} f(\varepsilon_\alpha + U_{\alpha n}), \tag{2}$$

and

$$\Gamma^-_{\alpha n} = \gamma_{\alpha n}[1 - f(\varepsilon_\alpha + U_{\alpha n})], \tag{3}$$

where $f(x) = \{\exp[(x-\mu_\alpha)/(k_B T_\alpha)] + 1\}^{-1}$ is the Fermi distribution, k_B is the Boltzmann constant, and $\gamma_{\alpha n}$ are the bare tunneling rate between the quantum dots and each of the reservoirs. The capacitances associated with each tunnel junction are defined by the charging energies $U_{\alpha n}$ of quantum dot α ($\alpha = s,g$), depending on whether the other quantum dot is empty ($n = 0$) or occupied ($n = 1$). The charging energies are, respectively, given by [24]

$$U_{s0} = \frac{q}{C\tilde{C}}\left(\frac{q}{2}C_{\Sigma g} + C_{\Sigma g}\sum_{s=l,r} C_s V_s + C C_g V_g\right), \tag{4}$$

$$U_{g0} = \frac{q}{C\tilde{C}}\left(\frac{q}{2}C_{\Sigma s} + C_{\Sigma s} C_g V_g + C\sum_{s=l,r} C_s V_s\right), \tag{5}$$

$$U_{s1} = U_{s0} + U, \tag{6}$$

and

$$U_{g1} = U_{g0} + U, \tag{7}$$

where $U = U_{\alpha 1} - U_{\alpha 0} = 2q^2/\tilde{C}$ is the exchanged energy between the two systems when an electron tunnels into the empty system but leaves it only after a second electron has occupied the other quantum dot, q is the elementary charge, and $V_{s/g} = \mu_{s/g}/q$ is the electric potential of the reservoirs s/g. The total capacitance of each quantum dot is defined by $C_{\Sigma s} = C_l + C_r + C$ or $C_{\Sigma g} = C_g + C$, and the effective capacitance $\tilde{C} = (C_{\Sigma s} C_{\Sigma g} - C^2)/C$.

In the steady-state, i.e., $\dot{p}_{n_s n_g} = 0$, the solutions of the occupation probability are as follows:

$$p_{00} = \frac{1}{\Omega}(\Gamma^+_{s1}\Gamma^-_{g1}\Gamma^-_{s0} + \Gamma^-_{g0}\Gamma^-_{g1}\Gamma^-_{s0} + \Gamma^-_{g0}\Gamma^+_{g1}\Gamma^-_{s1} + \Gamma^-_{g0}\Gamma^-_{s0}\Gamma^-_{s1}), \tag{8}$$

$$p_{10} = \frac{1}{\Omega}(\Gamma^+_{g0}\Gamma^+_{s1}\Gamma^-_{g1} + \Gamma^+_{s0}\Gamma^+_{s1}\Gamma^-_{g1} + \Gamma^+_{s0}\Gamma^-_{g0}\Gamma^-_{g1} + \Gamma^+_{s0}\Gamma^-_{g0}\Gamma^-_{s1}), \tag{9}$$

$$p_{01} = \frac{1}{\Omega}(\Gamma^+_{g1}\Gamma^+_{s0}\Gamma^-_{s1} + \Gamma^+_{g0}\Gamma^-_{g1}\Gamma^-_{s0} + \Gamma^+_{g0}\Gamma^+_{g1}\Gamma^-_{s1} + \Gamma^+_{g0}\Gamma^-_{s0}\Gamma^-_{s1}), \tag{10}$$

and

$$p_{11} = \frac{1}{\Omega}(\Gamma^+_{g0}\Gamma^+_{s1}\Gamma^+_{g1} + \Gamma^+_{s0}\Gamma^+_{s1}\Gamma^+_{g1} + \Gamma^+_{s0}\Gamma^-_{g0}\Gamma^+_{g1} + \Gamma^-_{s0}\Gamma^+_{g0}\Gamma^+_{s1}), \tag{11}$$

where Ω is the normalization factor that ensures the sum of probabilities to be equal to unity.

According to Eqs. (8)–(11), the charge currents from the quantum dot system to the left- (l) and right-side (r) reservoirs are, respectively, given by

$$I_l = q(\Gamma^-_{l0}p_{10} - \Gamma^+_{l0}p_{00} + \Gamma^-_{l1}p_{11} - \Gamma^+_{l1}p_{01}) \tag{12}$$

and

$$I_r = q(\Gamma^-_{r0}p_{10} - \Gamma^+_{r0}p_{00} + \Gamma^-_{r1}p_{11} - \Gamma^+_{r1}p_{01}). \tag{13}$$

In the steady state, the magnitude of charge currents I_r and I_l is the same but their directions are opposite, i.e., $I_l = -I_r \equiv I$. The total absorbing heat flow from the reservoir g is given by

$$\dot{Q}_g = (\varepsilon_g + U_{g0} - \mu_g)(\Gamma^+_{g0}p_{00} - \Gamma^-_{g0}p_{01}) + (\varepsilon_g + U_{g1} - \mu_g)(\Gamma^+_{g1}p_{10} - \Gamma^-_{g1}p_{11}). \tag{14}$$

III. CHARGE CURRENTS AND HEAT FLOWS

Based on Eqs. (12) and (13), the charge current I ($= I_l = -I_r$) from the right- (r) to left-side (l) reservoir may recast an expression as

$$I = \frac{I_{\rm abs} + I_{\rm rej}}{2}, \tag{15}$$

where $I_{\rm abs}$ and $I_{\rm rej}$ denote the contribution to the charge currents for the absorbing heat process from the reservoir g and the rejecting heat process to the reservoir g, respectively, and are given by

$$I_{\rm abs} = q(\Gamma^+_{r0}p_{00} - \Gamma^-_{r0}p_{10} + \Gamma^-_{l1}p_{11} - \Gamma^+_{l1}p_{01}) \tag{16}$$

and

$$I_{\rm rej} = q(\Gamma^-_{l0}p_{10} - \Gamma^+_{l0}p_{00} + \Gamma^+_{r1}p_{01} - \Gamma^-_{r1}p_{11}). \tag{17}$$

There is no energy exchange between the reservoir s and the reservoir g for the processes $\Gamma^{\pm}_{r0}$ or $\Gamma^{\pm}_{l0}$, but the processes $\Gamma^{\pm}_{l1}$ or $\Gamma^{\pm}_{r1}$ to transfer a particle from the right to left side must absorb or reject an energy U from or to the reservoir g. Thus, the heat flow absorbed from the reservoir g is given by

$$\dot{Q}_{\rm abs} = U(\Gamma^-_{l1}p_{11} - \Gamma^+_{l1}p_{01}) \tag{18}$$

and the heat flow rejected to the reservoir g is given by

$$\dot{Q}_{\rm rej} = U(\Gamma^+_{r1}p_{01} - \Gamma^-_{r1}p_{11}), \tag{19}$$

so that

$$\dot{Q}_g = \dot{Q}_{\rm abs} - \dot{Q}_{\rm rej}. \tag{20}$$

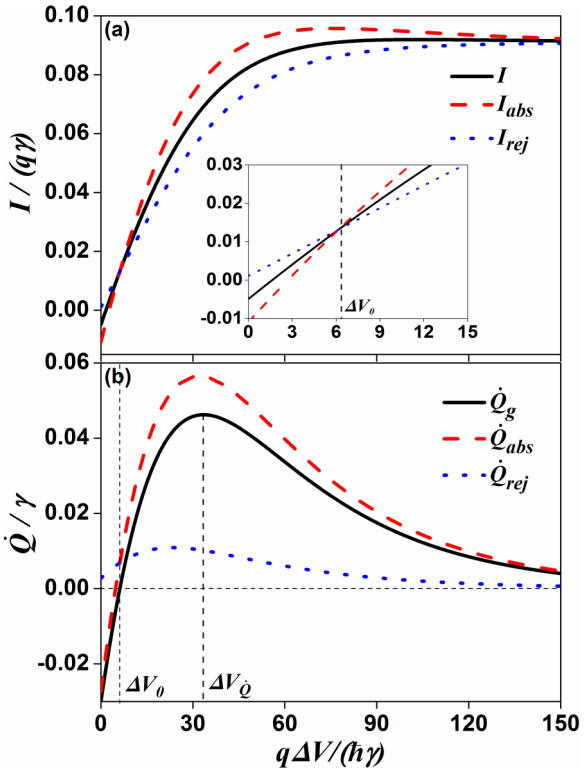

FIG. 2. (Color online) Charge currents I and heat flows $\dot{Q}$ as a function of the voltage bias for $\lambda = 0.1$. Inset (a): the partial enlarged detail.

In what follows, it is assumed that $T_l = T_r \equiv T_s$. A set of physically reasonable parameters are adopted in following calculations, i.e., $k_B T_l = k_B T_r = k_B T_s = 2k_B T_g$, $k_B T_g = 5\hbar\gamma$, $q^2/C_\alpha = 20\hbar\gamma$, $q^2/C = 50\hbar\gamma$, $\varepsilon_\alpha = \varepsilon_g = 0$, and $\gamma_{\alpha n} = \gamma$, except $\gamma_{l0} = \gamma_{r1} = \lambda\gamma$ ($0 \leqslant \lambda \leqslant 1$), where $\hbar$ is the reduced Planck constant and λ is defined as the dissipation factor.

The curves of charge currents I (I, $I_{\rm abs}$, and $I_{\rm rej}$) and heat flows $\dot{Q}$ ($\dot{Q}_c$, $\dot{Q}_{\rm abs}$, and $\dot{Q}_{\rm rej}$) as a function of the voltage bias ΔV for $\lambda = 0.1$ are plotted, as shown in Figs. 2(a) and 2(b). We note that $I_{\rm abs} = I_{\rm rej}$ and $\dot{Q}_{\rm abs} = \dot{Q}_{\rm rej}$ are obtained for $\Delta V = \Delta V_0$. At this point, the charge current $I_{\rm abs}$ (the absorbing heat process), mainly driven by the voltage bias, and the charge current $I_{\rm rej}$ (the rejecting heat process), mainly powered by the temperature gradient, compensate each other. In the case of $\Delta V > \Delta V_0$, the charge currents always keep $I_{\rm abs} > I_{\rm rej}$, and the heat flow $\dot{Q}_{\rm abs} > \dot{Q}_{\rm rej}$. But in the limit of $\Delta V \gg 0$, charge currents $I_{\rm abs}$ and $I_{\rm rej}$tend to be equal and will maintain a constant, so that $\dot{Q}_g (= \dot{Q}_{\rm abs} - \dot{Q}_{\rm rej}) \to 0$. Thus, there is a maximum for every of heat flows $\dot{Q}$ ($\dot{Q}_c$, $\dot{Q}_{\rm abs}$, and $\dot{Q}_{\rm rej}$) at

the voltage bias $\Delta V_{\dot{Q}}$. This is because that the charge current I consists of two parts $I_{\rm abs}$ and $I_{\rm rej}$, and the processes $\Gamma^{\pm}_{r0}$ and $\Gamma^{\pm}_{l1}$ or $\Gamma^{\pm}_{l0}$ and $\Gamma^{\pm}_{r1}$ contributes to the currents $I_{\rm abs}$ or $I_{\rm rej}$ at the same time. But the processes $\Gamma^{\pm}_{r0}$ or $\Gamma^{\pm}_{l0}$ have no contribution for energy transmission, as shown in Eqs. (15)–(19), so that the processes $\Gamma^{\pm}_{l1}$ or $\Gamma^{\pm}_{r1}$ play a main role to transfer energy between the reservoirs when $\Delta V < \Delta V_{\dot{Q}}$. But in the case of $\Delta V > \Delta V_{\dot{Q}}$, the processes $\Gamma^{\pm}_{r0}$ or $\Gamma^{\pm}_{l0}$ of no energy exchange are more and more significant, so heat flows $\dot{Q}$ ($\dot{Q}_c$, $\dot{Q}_{\rm abs}$, and $\dot{Q}_{\rm rej}$) gradually decreases as the voltage bias increases. Especially, for very small bias voltage $\Delta V < \Delta V_0$, $I_{\rm abs} < I_{\rm rej}$, and $\dot{Q}_{\rm abs} < \dot{Q}_{\rm rej}$, so that the total heat flow $\dot{Q}_g$ absorbed from the reservoir g is negative. This is mainly because the heat flow of the absorbing heat process driven by the voltage bias is not enough to offset that of the rejecting heat process powered by temperature gradient.

In Fig. 3, we show the calculation results of charge currents (a) and heat flows (b) as a function of the dissipation factor λ. There exists a special point λ_s, leading to $I_{\rm abs} = I_{\rm rej}$ and $\dot{Q}_{\rm abs} = \dot{Q}_{\rm rej}$, so that the total absorbing heat flow $\dot{Q}_g = 0$. In the case of $\lambda < \lambda_s$, $I_{\rm abs} > I_{\rm rej}$, and $\dot{Q}_{\rm abs} > \dot{Q}_{\rm rej}$, so that $\dot{Q}_g > 0$. This kind of circumstance can realize refrigeration for the reservoir g. But in the case of $\lambda > \lambda_s$, it leads to $I_{\rm abs} < I_{\rm rej}$ and $\dot{Q}_{\rm abs} < \dot{Q}_{\rm rej}$, so that $\dot{Q}_g < 0$. This kind of situation is undesired in the following discussion. It is seen from Fig. 3(b) that the total absorbing heat flow $\dot{Q}_g$ gradually decreases with the increase of the dissipation factor λ. Therefore, the parameter λ is defined as the dissipation factor.

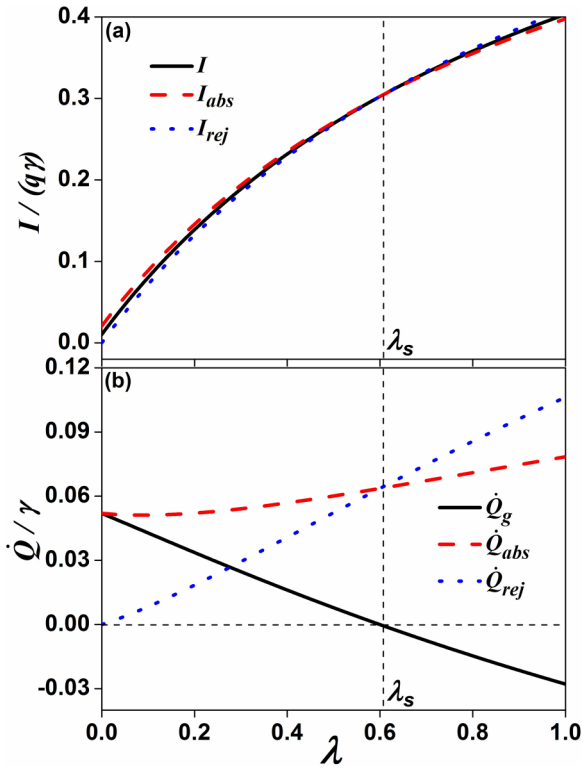

FIG. 3. (Color online) The curves of charge currents I and heat flows $\dot{Q}$ varying with the dissipation factor λ for $q\Delta V/(\hbar\gamma) = 45$.

IV. PERFORMANCE EVALUATION OF A REFRIGERATOR

A. Performance characteristics

We first consider the case of $T_s > T_g$. Such a system can constitute a refrigerator to cool the reservoir g. The heat flow $\dot{Q}_g$ is absorbed from the reservoir g by the applied bias voltage $\Delta V = (\mu_r - \mu_l)/q$, and the heat flow $\dot{Q}_s$ is rejected to the reservoir s. According to the first law of thermodynamics, $\dot{Q}_g + P = \dot{Q}_s$, where $P = I\Delta V$ is the power input. Thus, the cooling power $\dot{Q}_c$ is given by $\dot{Q}_c = \dot{Q}_g$ and the coefficient of performance (COP) is defined as

$$\varepsilon = \frac{\dot{Q}_c}{P} = \frac{\dot{Q}_g}{P}. \tag{21}$$

In the limiting case of $\lambda = 0$, the contribution of the undesired processes (the processes $\Gamma^{\pm}_{r1}$ and $\Gamma^{\pm}_{l0}$ reject an energy U to the reservoir g) will be negligible. As a consequence, based on Eqs. (12) and (14), the charge current I and heat flow $\dot{Q}_g$ are related only by their quantization, namely

$$\frac{I}{\dot{Q}_g} = \frac{q}{U}. \tag{22}$$

This means that the energy transferred between the two systems (conductor and gate systems) is quantized: a charge current flowing along the conductor and an energy U transferring from the gate reservoir g into the conductor reservoirs s. Therefore, the COP is simplified as

$$\varepsilon = \frac{U}{q\Delta V}. \tag{23}$$

The COP is inversely proportional to the voltage bias and achieve the Carnot COP $\varepsilon_C = T_g/(T_s - T_g)$ at the threshold voltage $\Delta V = \Delta V_0 = U/(q\varepsilon_C)$, but the cooling power $\dot{Q}_c$ will vanish, as shown in Fig. 4.

Figure 4 shows the performance characteristics of the three-terminal quantum-dot refrigerator. It is seen from Fig. 4(a) that the cooling power increases first and then decreases as the voltage bias increases for a given λ. There exists an optimum voltage bias $\Delta V_{\dot{Q}_c}$ leading to a maximum cooling power $\dot{Q}_c^{\rm max}$. On the other hand, the maximum cooling power $\dot{Q}_c^{\rm max}$decrease gradually with the increase of the dissipation factor. Figure 4(b) shows that the COP is a nonmonotonous function of the voltage bias for given values of $\lambda \neq 0$. There exists an optimum voltage bias ΔV_ε leading to a maximum COP $\varepsilon_{\rm max}$. In the region of $\Delta V < \Delta V_\varepsilon$, the COP increases as the voltage bias increases. While in the region of $\Delta V > \Delta V_\varepsilon$, the COP decreases as the voltage bias increases. It is seen that the maximum COP decreases rapidly with the increase of λ. Particularly, there exists a threshold voltage ΔV_0. The system can realize the refrigeration only when the voltage bias is greater than the threshold voltage. In addition, for the case of $\lambda = 0$, the cooling power vanishes when the voltage bias arrives at the so called the threshold voltage ΔV_0, because the electric current is equal to zero. At this point, the COP can achieve its maximum value, which means that the refrigerator works at nondissipative situation.

By using the data in Figs. 4(a) and 4(b), the characteristic curves of the cooling power versus COP can be plotted, as shown in Fig. 4(c). Due to the contribution of these undesired processes $\Gamma^{\pm}_{r1}$ and $\Gamma^{\pm}_{l0}$ can be negligible for the case of

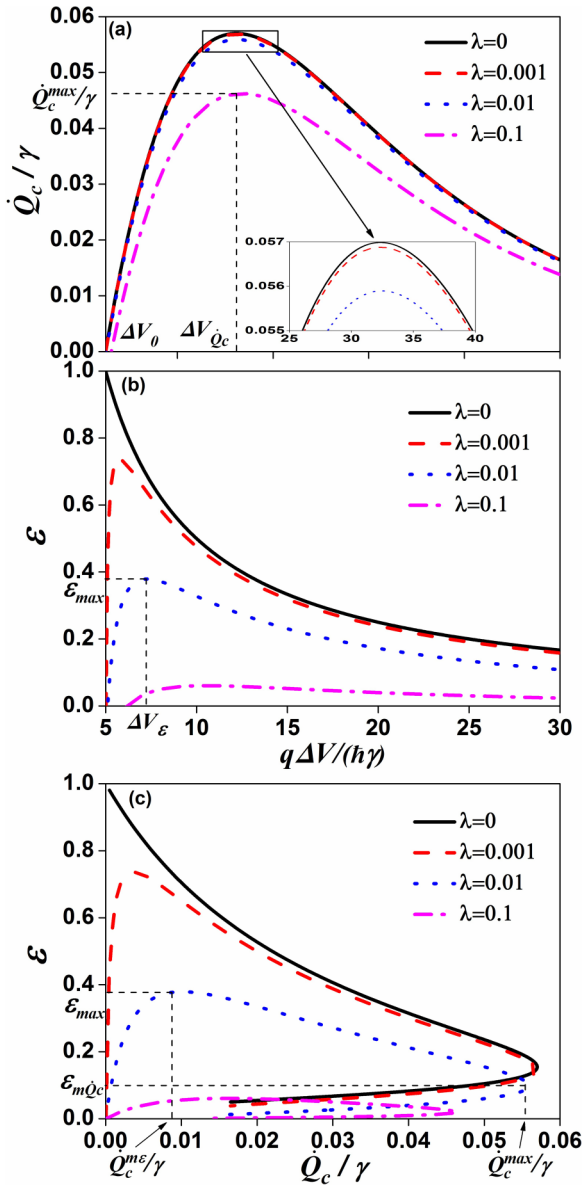

FIG. 4. (Color online) Performance characteristics of a three-terminal quantum-dot refrigerator. (a) The cooling power and (b) the coefficient of performance as a function of the voltage bias for different values of the dissipation factor λ. (c) Characteristic curves for different values of dissipation factor λ. Inset (a): the partial enlarged detail.

$\lambda = 0$, the electronic transport is ideal and of no dissipation. Therefore, it is seen that the characteristic curve between the cooling power and the COP is open shaped. But, for the case of $\lambda \neq 0$, the electronic transport of these undesired processes will gradually increase with the increase of λ. Therefore, the characteristic curves are closed loop-shaped. This means that the cooling power at the maximum COP does not vanish.

For actual refrigerators, engineers always want to get a COP as large as possible and at the same time obtain one large cooling power. Therefore, the optimally operating regions of the quantum dot refrigerator should be located in those regions of the $\varepsilon \sim \dot{Q}$ curves with negative slopes, as shown in Fig. 4(c). Thus, the optimal regions of the three-terminal quantum-dot refrigerator should be

$$\dot{Q}_c^{m\varepsilon} \leqslant \dot{Q} \leqslant \dot{Q}_c^{\max}, \tag{24}$$

and

$$\varepsilon_{m\dot{Q}_c} \leqslant \varepsilon \leqslant \varepsilon_{\max}, \tag{25}$$

where $\dot{Q}_c^{me}$, $\dot{Q}_c^{\max}$, $\varepsilon_{m\dot{Q}_c}$, and $\varepsilon_{\max}$ are four important parameters which determine the lower and upper bounds of the optimized cooling power and COP of a quantum-dot refrigerator.

B. Performance optimization

The variation curves of the threshold voltage ΔV_0 and the optimal voltage biases $\Delta V_{\dot{Q}_c}$ and ΔV_ε at the maximum cooling power and maximum COP as a function of the dissipation factor λ are plotted as shown in Fig. 5. It is found that the threshold voltage increases rapidly with the increase of the dissipation factor and reaches infinite at the maximum dissipation factor $\lambda_{\max} \approx 0.608$. This means that the dissipation tunneling processes $\Gamma_{r1}^{\pm}$ and $\Gamma_{l0}^{\pm}$ are greater than the refrigeration transport process $\Gamma_{r0}^{\pm}$ and $\Gamma_{l1}^{\pm}$. Therefore, in the actual design, the operating regions of the dissipation factor λ should be $0 < \lambda < \lambda_{\max}$. Moreover, it is found that the optimal region of the voltage bias should be

$$\Delta V_\varepsilon \leqslant \Delta V \leqslant \Delta V_{\dot{Q}_c}, \tag{26}$$

as shown in the gray area in Fig. 5. Obviously, ΔV_ε and $\Delta V_{\dot{Q}_c}$ are also two important parameters that determine the lower and upper bounds of the optimized voltage bias. In this optimal voltage bias region, the quantum-dot refrigerator is located in the range of the characteristic curves with negative slopes. The optimal voltage bias regions gradually decrease with the increase of λ. The results obtained here indicate a way to operate the refrigerator at the optimum ranges.

The curves of the maximum cooling power varying with the temperature ratio T_g/T_s are plotted for different values of λ, as shown in Fig. 6(a). It is clearly shown that the maximum cooling power is a monotonically increasing function of T_g/T_s and gradually decreases with the increase of the dissipation factor λ. The COP at the maximum cooling power in the

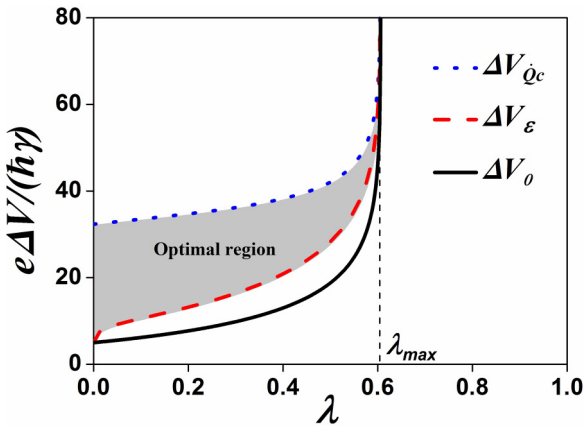

FIG. 5. (Color online) The threshold voltage (solid line) and optimal voltage biases at the maximum cooling power (blue dot line) and maximum COP (red dash line) as a function of the dissipation factor λ.

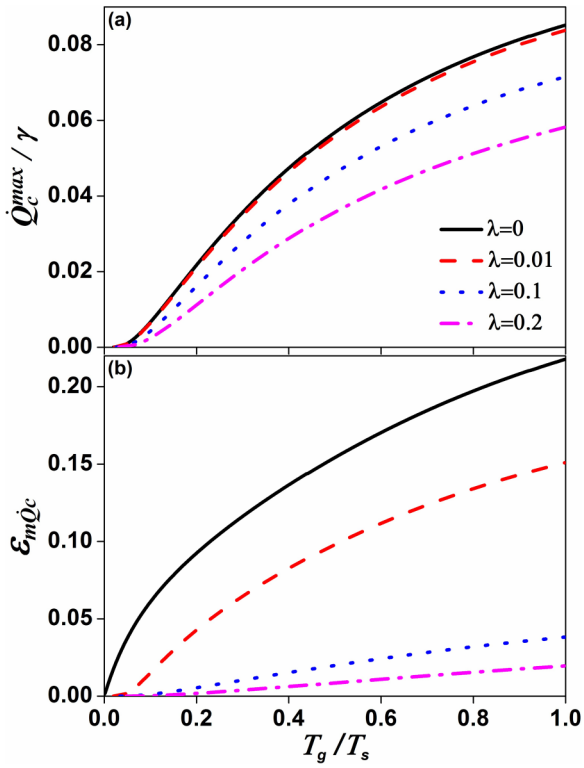

FIG. 6. (Color online) (a) The maximum cooling power and (b) the COP at the maximum cooling power as a function of the temperature ratio T_g/T_s for different values of the dissipation factor λ.

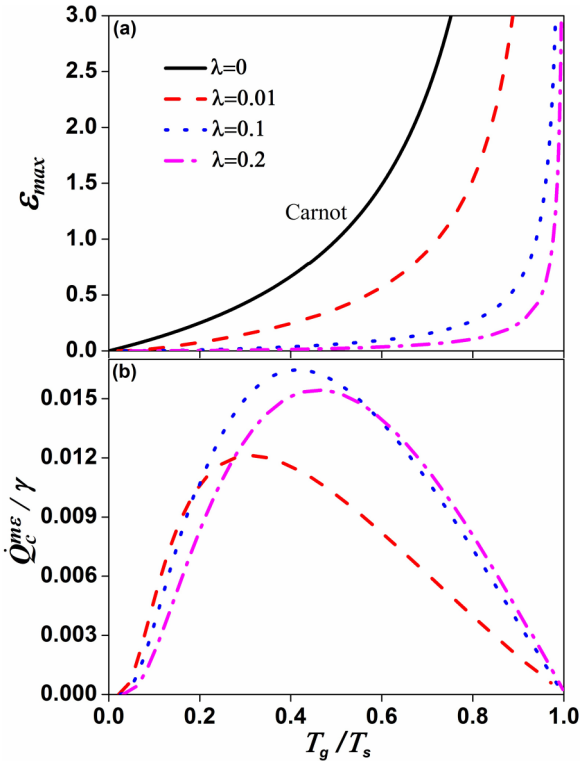

FIG. 7. (Color online) (a) The maximum COP and (b) the cooling power at the maximum COP as a function of the temperature ratio T_g/T_s for different values of the dissipation factor λ.

dissipation cases ($\lambda \neq 0$) is smaller than that in the ideal case ($\lambda = 0$) and obviously decreases as the dissipation factor λ increases, as shown in Fig. 6(b).

Figure 7 shows (a) the maximum COP and (b) the corresponding cooling power as a function of the temperature ratio T_g/T_s for different values of the dissipation factor λ. It is seen that the maximum COP decreases as the dissipation factor λ increases. For the case of $\lambda = 0$, the maximum COP is equal to the Carnot COP, i.e., $\varepsilon_{\max} = \varepsilon_C$, but the corresponding cooling power is zero. While the corresponding cooling power increases first and then decreases as the dissipation factor λ increases. Therefore, the dissipation factor λ has an optimal value at which the cooling power at the maximum COP will attains its maximum. This will be discussed hereinafter.

Figure 8 shows the maximum cooling power and the corresponding COP at the maximum cooling power as a function of the dissipation factor λ. It is found that for the case of $\lambda = 0$, maximum cooling power and the corresponding COP reach their maximum value. But, for the case of $\lambda \neq 0$, both the maximum cooling power and the corresponding COP obviously decrease as the dissipation factor λ increases. When the maximum dissipation factor $\lambda = \lambda_{\max}$, $\dot{Q}_c^{\max} = 0$, and $\varepsilon_{m\dot{Q}_c} = 0$, because the undesired processes $\Gamma_{r1}^{\pm}$ and $\Gamma_{l0}^{\pm}$ cannot be negligible. Hence, these undesired processes $\Gamma_{r1}^{\pm}$ and $\Gamma_{l0}^{\pm}$ should be minimized as largely as possible in the actual maximum cooling power optimization design.

The variation curves of the maximum COP and corresponding cooling power at the maximum COP with the dissipation factor λ are plotted as shown in Fig. 9. It is seen that the maximum COP decreases as the dissipation factor λ increases, while the corresponding cooling power at the maximum COP increases first and then decreases as the dissipation factor λ increases, yielding to its maximum value $\dot{Q}_c^{m\varepsilon}/\gamma \approx 0.0161$ at $\lambda_{\text{opt}} \approx 0.114$. It shows that the maximum COP optimization is different from the maximum cooling power optimization. In order to achieve the maximum COP and at the same time obtain a large cooling power, the quantum-dot refrigerator should work in the area of $\lambda \leqslant \lambda_{\text{opt}}$, as shown in Fig. 9. Thus, in the actual design, the optimal region of the dissipation factor

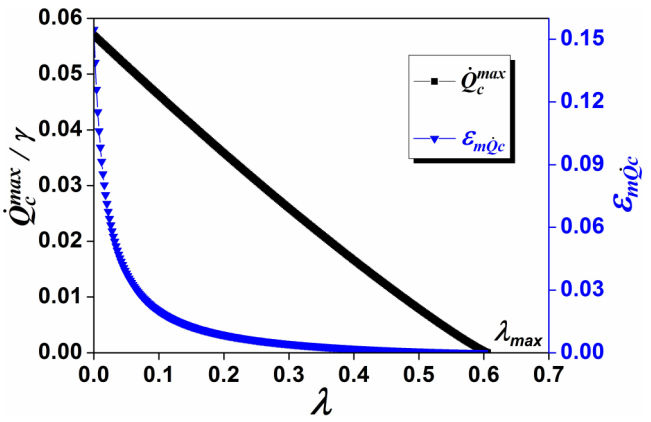

FIG. 8. (Color online) The maximum cooling power (black line) and the COP at the maximum cooling power (blue line) as a function of the dissipation factor λ.

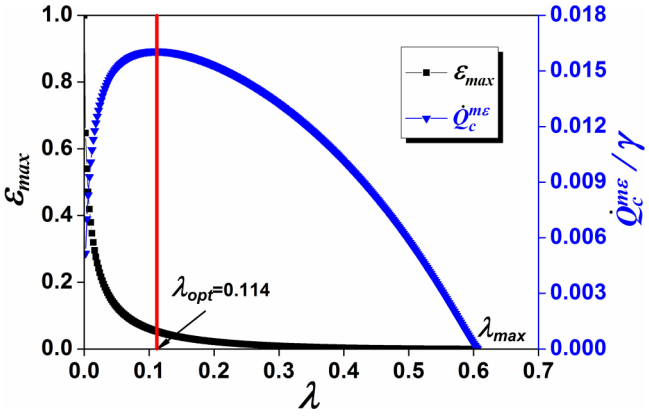

FIG. 9. (Color online) The maximum COP (black line) and the cooling power at the maximum COP (blue line) as a function of the dissipation factor λ.

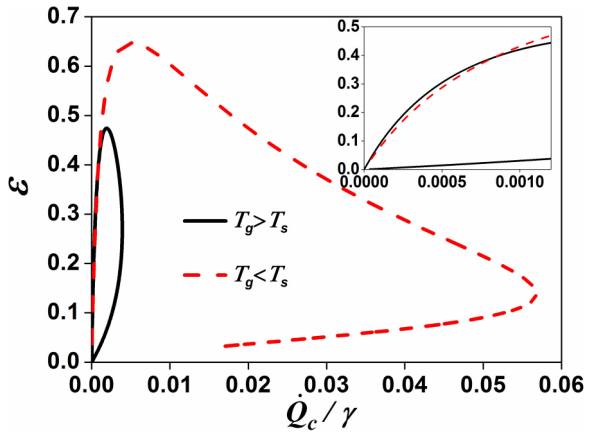

FIG. 10. (Color online) The characteristic curves of the refrigerators in the cases of $T_g > T_s$ and $T_s > T_g$ for $\lambda = 0.002$. Inset: the partial enlarged detail.

λ should be $0 < \lambda \leqslant \lambda_{\rm opt}$. According to this criterion, Eq. (26) may be rewritten as $\Delta V_\varepsilon(\lambda = 0) \leqslant \Delta V \leqslant \Delta V_{\dot{Q}_c}(\lambda = \lambda_{\rm opt})$.

C. Discussion and comparison

We now turn to discuss the performance of the refrigerator operated in the case of $T_g > T_s$, which has the same initial configuration as in the previous case, except parameters $k_B T_s = 5\hbar\gamma$, $T_g = 2T_s$, and $\gamma_{l1} = \gamma_{r0} = \lambda\gamma$ $(0 \leqslant \lambda \leqslant 1)$. The results obtained will be compared with those of the refrigerator operated in the case of $T_s > T_g$.

In the case of $T_g > T_s$, the heat flow $-\dot{Q}_s$ absorbed from the reservoir s by the applied bias voltage $\Delta V = (\mu_r - \mu_l)/q$, and the heat flow $-\dot{Q}_g$ rejected to the reservoir g. Hence, according to the first law of thermodynamics is $-\dot{Q}_g = P - \dot{Q}_s$. Thus, the cooling power $\dot{Q}_c$ is given by $\dot{Q}_c = -\dot{Q}_s$, and the COP is defined as

$$\varepsilon = \frac{-\dot{Q}_s}{P} = \frac{-\dot{Q}_g - P}{P}. \tag{27}$$

In the case of $\lambda = 0$, we get $I/-\dot{Q}_g = q/U$, which is similar to the previous case. Therefore, Eq. (27) is simplified as

$$\varepsilon = \frac{U - q\Delta V}{q\Delta V}. \tag{28}$$

The Carnot COP $\varepsilon_C = T_s/(T_g - T_s)$ can be achieved at the threshold voltage $\Delta V = \Delta V_0 = U/[q(\varepsilon_c + 1)]$. In particular, the COP vanishes, i.e., $\varepsilon = 0$, at the so-called stopping voltage $\Delta V_{\rm stop} = U/q$. This is mainly due to the quantization of the charge current and heat flow. In every state of the cycle processes shown in Fig. 1(b), a certain energy U not depending on the voltage bias is transferred. Thus, in the case of $T_g > T_s$, the range of the voltage bias must be

$$U/[q\,(\varepsilon_c + 1)] \equiv \Delta V_0 < \Delta V < \Delta V_{\rm stop} \equiv U/q. \tag{29}$$

The characteristic curves of the cooling power versus COP can be plotted as shown in Fig. 10. Due to all the heat flow $\dot{Q}_g$ absorbed from the reservoir g by the applied voltage bias contribute to the cooling power in the case of $T_s > T_g$, but in the case of $T_g > T_s$, the heat flow $\dot{Q}_g$ rejected by the reservoir g consists of two parts, where one part comes from the power input and the other part comes from the cooling power. It is found that the cooling power in the case of $T_g > T_s$ is significantly smaller than that in the case of $T_s > T_g$. However, in the region where the cooling power is very small, the COP in the case of $T_g > T_s$ is slightly greater than that in the case of $T_s > T_g$, as shown by the inset of Fig. 10. But, in the optimal region that the $\varepsilon \sim \dot{Q}$ curves with negative slopes, both the cooling power and COP in the case of $T_g > T_s$ are smaller than those in the case of $T_s > T_g$. Thus, the refrigerator operated in the case of $T_g > T_s$ should not be adopted in practical applications.

Figure 11 shows the maximum COPs as a function of the temperature ratio τ ($\tau = T_s/T_g$ for $T_g > T_s$, $\tau = T_g/T_s$ for $T_s > T_g$). It is found that the temperature ratio τ must be larger than the threshold temperature ratio τ_0' in the case of $T_g > T_s$ (τ_0 in the case of $T_s > T_g$, as shown by the inset of Fig. 11). This is because the heat flow driven by temperature difference is larger than that driven by the voltage bias. When the temperature ratio $\tau \leqslant \tau_0'$ in the case of $T_g > T_s$ (τ_0 in the case of $T_s > T_g$), the refrigerator will lose its role. Because $\tau_0 < \tau_0'$, it shows once again that in practical applications, one should adopt

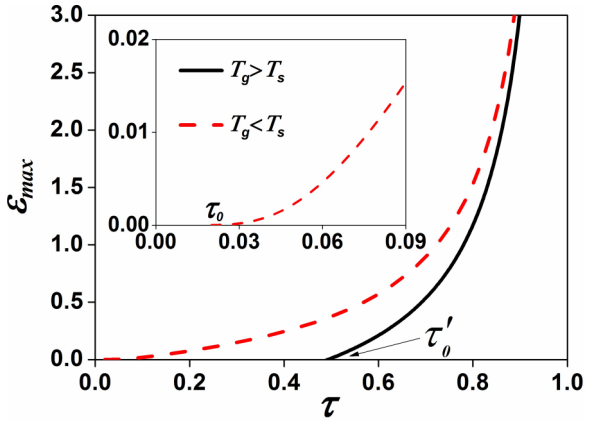

FIG. 11. (Color online) The maximum COPs as a function of the temperature ratio τ in the cases of $T_g > T_s$ and $T_s > T_g$ for $\lambda = 0.01$. Inset: the partial enlarged detail.

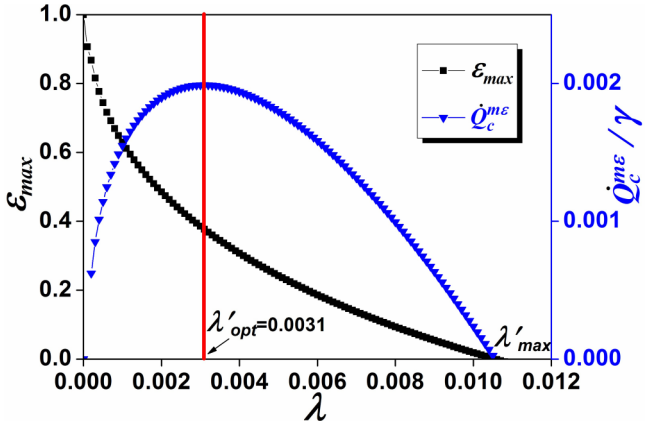

FIG. 12. (Color online) The maximum COP (black line) and the cooling power at the maximum COP (blue line) as a function of the dissipation factor λ.

the refrigerator operated in the case of $T_s > T_g$ rather than $T_g > T_s$.

The variation curves of the maximum COP and the cooling power at the maximum COP with the dissipation factor λ are plotted as shown in Fig. 12. It is seen that the maximum dissipation factor $\lambda'_{\max} \approx 0.0106$ in the case of $T_g > T_s$. Compared with the case of $T_s > T_g$ shown in Fig. 9, it is found that $\lambda'_{\max} < \lambda_{\max}$. The cooling power at the maximum COP can reaches its maximum value $(\dot{Q}_c^{m\varepsilon}/\gamma)^* \approx 0.00199$ at $\lambda'_{\rm opt} = 0.0031$. It is found that both the maximum cooling power at the maximum COP and optimal dissipation factor in the case of $T_g > T_s$ is significantly smaller than those in the case of $T_s > T_g$, i.e., $(\dot{Q}_c^{m\varepsilon}/\gamma)^* < \dot{Q}_c^{m\varepsilon}/\gamma$ and $\lambda'_{\rm opt} < \lambda_{\rm opt}$.

V. CONCLUSIONS

We have analyzed the thermodynamic performance characteristics of three-terminal quantum-dot refrigerators operated in two different cases. This study is based on the evaluation of the cooling power and COP derived from the steady-state charge and energy transport between two quantum dots and thermal reservoirs in the sequential tunneling approximation. It is found that when the dissipation factor is not equal to zero, the contribution of undesired processes is a major source of the irreversibility of three-terminal quantum-dot refrigerators. We have shown that the Carnot COP can be achieved in the limiting case that the dissipation factor is equal to zero. The optimally operating regions of three-terminal quantum-dot refrigerators should be located in the characteristic curves with negative slopes. Therefore, quantum-dot refrigerators can be operated at the optimal regime by reasonably choosing the system's parameters. For the actual refrigeration system, the optimal region of the voltage bias should be $\Delta V_\varepsilon(\lambda = 0) \leqslant \Delta V \leqslant \Delta V_{\dot{Q}_c}(\lambda = \lambda_{\rm opt})$. In order to achieve simultaneously a high COP and a large cooling power, the dissipation factor λ should be chosen in the range of $0 < \lambda \leqslant \lambda_{\rm opt}$ in the case of $T_s > T_g$. Through the comparison of the performance characteristics of the refrigerators operated in the case of $T_s > T_g$ and $T_g > T_s$, it is found that both the cooling power and maximum COP in the case of $T_g > T_s$ are smaller than those in the case of $T_s > T_g$, and that the refrigerator operated in the case of $T_g > T_s$ should not be adopted in practical applications. The results obtained here show that the investigation on the optimal performance of three-terminal quantum-dot refrigerators is very necessary and is not the simple duplicate research on the performance of three-terminal quantum-dot heat engines. They may fill the existing gap in the field of three-terminal quantum-dot thermoelectric devices and provide some theoretical guidelines for the optimal design and manipulate of practical three-terminal quantum-dot refrigerators.

ACKNOWLEDGMENT

This work has been supported by the National Natural Science Foundation (Grant No. 11175148), People's Republic of China.

[1] G. J. Snyder and E. S. Toberer, Nat. Mater. **7**, 105 (2008).
[2] P. Pichanusakorn and P. Bandaru, Mater. Sci. Eng. R **67**, 19 (2010).
[3] G. Mahan, B. Sales, and J. Sharp, Phys. Today **50**, 42 (1997).
[4] F J. DiSalvo, Science **285**, 703 (1999).
[5] L. D. Hicks and M. S. Dresselhaus, Phys. Rev. B **47**, 12727 (1993).
[6] L. D. Hicks and M. S. Dresselhaus, Phys. Rev. B **47**, 16631 (1993).
[7] G. D. Mahan and J. O. Sofo, Proc. Natl. Acad. Sci. USA **93**, 7436 (1996).
[8] T. E. Humphrey, R. Newbury, R. P. Taylor, and H. Linke, Phys. Rev. Lett. **89**, 116801 (2002).
[9] T. E. Humphrey and H. Linke, Phys. Rev. Lett. **94**, 096601 (2005).
[10] M. Esposito, K. Lindenberg, and C. Van den Broeck, Europhys. Lett. **85**, 60010 (2009).
[11] M. Esposito, R. Kawai, K. Lindenberg, and C. Van den Broeck, Phys. Rev. E **81**, 041106 (2010).
[12] M. Esposito, N. Kumar, K. Lindenberg, and C. Van den Broeck, Phys. Rev. E **85**, 031117 (2012).
[13] Y. C. Zhang and J. Z. He, Chin. Phys. Lett. **30**, 010501 (2013).
[14] Y. C. Zhang, J. Z. He, X. He, and Y. L. Xiao, Phys. Scr. **88**, 035002 (2013).
[15] C. Li, Y. C. Zhang, J. H. Wang, and J. Z. He, Phys. Rev. E **88**, 062120 (2013).
[16] S. F. Godijn, S. Möller, H. Buhmann, L. W. Molenkamp, and S. A. van Langen, Phys. Rev. Lett. **82**, 2927 (1999).
[17] M. C. Llaguno, J. E. Fischer, A. T. Johnson, and J. Hone, Nano Lett. **4**, 45 (2003).
[18] A. A. M. Staring, L. W. Molenkamp, B. W. Alphenaar, H. van Houten, O. J. A. Buyk, M. A. A. Mabesoone, C. W. J. Beenakker, and C. T. Foxon, Europhys. Lett. **22**, 57 (1993).
[19] L. Molenkamp, A. A. M. Staring, B. W. Alphenaar, H. van Houten, and C. W. J. Beenakker, Semicond. Sci. Technol. **9**, 903 (1994).
[20] A. S. Dzurak, C. G. Smith, C. H. W. Barnes, M. Pepper, L. Martín-Moreno, C. T. Liang, D. A. Ritchie, and G. A. C. Jones, Phys. Rev. B **55**, R10197 (1997).

[21] H. L. Edwards, Q. Niu, and A. L. de Lozanne, Appl. Phys. Lett. **63**, 1815 (1993).
[22] H. L. Edwards, Q. Niu, G. A. Georgakis, and A. L. de Lozanne, Phys. Rev. B **52**, 5714 (1995).
[23] J. R. Prance, C. G. Smith, J. P. Griffiths, S. J. Chorley, D. Anderson, G. A. C. Jones, I. Farrer, and D. A. Ritchie, Phys. Rev. Lett. **102**, 146602 (2009).
[24] R. Sánchez and M. Büttiker, Phys. Rev. B **83**, 085428 (2011).
[25] J. P. Pekola, J. V. Koski, and D. V. Averin, Phys. Rev. B **89**, 081309(R) (2014).
[26] I. H. Chan, R. M. Westervelt, K. D. Maranowski, and A. C. Gossard, Appl. Phys. Lett. **80**, 1818 (2002).
[27] A. Hübel, J. Weis, W. Dietsche, and K. v. Klitzing, Appl. Phys. Lett. **91**, 102101 (2007).
[28] E. Bonet, M. M. Deshmukh, and D. C. Ralph, Phys. Rev. B **65**, 045317 (2002).
[29] U. Harbola, M. Esposito, and S. Mukamel, Phys. Rev. B **74**, 235309 (2006).
[30] M. Esposito, K. Lindenberg, and C. Van den Broeck, Phys. Rev. Lett. **102**, 130602 (2009).